DEPARTMENT OF COMPUTER SCIENCE ENGINEERING,
SCHOOL OF ENGINEERING AND TECHNOLOGY,
SHARDA UNIVERSITY, GREATER NOIDA

LANE AND VEHICLE DETECTION USING HOUGH TRANSFORM AND YOLOv3

A project submitted
In partial fulfillment of the requirements for the degree of
Bachelor of Technology in Computer Science and Engineering

By

Subash Kumar Shah (2018000119)

Agrima Yadav (2018006287)

Kartikeya (2018007496)

Nikhil Gupta (2019006638)

Supervised by:

Mr. Sunil Kumar
Assistant Professor

May, 2022

CERTIFICATE

This is to certify that the report entitled "**Lane And Vehicle Detection Using Hough Transform And Yolov3** " submitted by "Subash Kumar Shah (180101334), Agrima Yadav (180101029), Kartikeya (180101147), Nikhil Gupta (190101097)" to Sharda University, towards the fulfillment of requirements of the degree of "Bachelor of Technology" is record of bonafide final year Project work carried out by him in the "Department of Computer Science and Engineering, School of Engineering and Technology, Sharda University".

The results/findings contained in this Project have not been submitted in part or full to any other University/Institute for award of any other Degree/Diploma.

Signature of Supervisor

Name: Mr. Sunil Kumar

Designation: Assistant Professor (CSE)

Signature of Head of Department

Name: Prof. (Dr.) Nitin Rakesh

Place:

Date:

Signature of External Examiner

Date:

ACKNOWLEDGEMENT

A major project is a golden opportunity for learning and self-development. We consider our self very lucky and honored to have so many wonderful people lead us through in completion of this project.

First and foremost, we would like to thank Dr. Nitin Rakesh, HOD, CSE who gave us an opportunity to undertake this project.

My grateful thanks to **Mr. Sunil Kumar, Assistant Professor** in CSE for their guidance in our project work. **Mr. Sunil Kumar, Assistant Professor**, who in spite of being extraordinarily busy with academics, took time out to hear, guide and keep us on the correct path. We do not know where we would have been without his help.

CSE department monitored our progress and arranged all facilities to make life easier. We choose this moment to acknowledge their contribution gratefully.

Name and signature of Students
Subash Kumar Shah (180101334)

Agrima Yadav (180101029)

Kartikeya (180101147)

Nikhil Gupta (190101097)

Abstract

Object tracking at dark is critical to minimizing the number of nocturnal traffic crashes. This paper presents a deep convolutional neural network dubbed YOLO to enhance the precision of nocturnal object recognition and to be suited for limited contexts (also including microcontrollers in automobiles). To begin, track line images are separated into other * 2S panels based on the features of uneven spatial and temporal dispersion densities. Additionally, the sensor frequency has been limited to four measurement levels, making it even more suited for tiny source localization, like lateral distance measurement. Thirdly, to optimize the connectivity, a fully connected layer throughout the basic Yolo v3 method is reduced by 53 to 49 levels. Lastly, characteristics like cluster center radius and backpropagation are enhanced. According to the testing data, while utilizing the enhanced recognition system for lane object tracking, the accurate prediction precision map figure is 92.03 percent and also the computing power is 48 frames per second. It outperforms the initial Yolo v3 method in terms of recognition rate and actual throughput.

A responsive road attribute deep learning model that can enable learning the properties of a track in different settings is suggested to enhance the precision of border recognition in complicated circumstances. The first step is to build a multiple training approach that relies on the YOLO v3 (You Only Look Once, v3) algorithm. The YOLO v3 method's geometrical properties are changed to make it highly appropriate for target tracking. A technique for continuous production of channel label pictures in a basic environment, which supplies specific information needed for such activation of the first-stage system, is presented to increase subsequent revisions. The track determined by the first-stage system would then be relocated using an ideal system technique to diagnose relying on the Canny activator. In addition, the unrecognized routes are protected to prevent disruption in even more feature learning. The photos analyzed mostly by preceding procedure are therefore utilized as label features to instruct the second- stage model. The testing was performed using the KITTI as well as Caltech records, and thus the findings demonstrated that the efficiency and effectiveness of the second - stage model had achieved an unprecedented level.

Index Terms Deep Learning, Vehicle Detection, Hough Transform, LaneRTD Algorithm, Canny Edge Sensor

Contents

List of Figures

Chapter 1: INTRODUCTION

Estimating vehicle flow factors are critical in the development, engineering, and management of comprehensive road infrastructures. Furthermore, Intelligent Transportation Systems (ITS) need the monitoring and regulation of travel times and flow velocity in legitimate with greater precision and efficiency than those in the prior [1]. Many concepts and tools are available for collecting traffic information, such as "static point assessment" (i.e., deductive approach, hydraulic pipes, sensors, camcorders, etc.) as well as "gauge automobile information" techniques (i.e., vehicle trajectory information FCD), which are both frequently utilized.

Numerous Deep Learning-based strategies may be used in static point measuring approaches for automobile tracking and identification procedures [2–5]. With the fast evolution of China's automotive sector as well as the constant advancement of machine learning systems in subsequent generations, automobiles with ancillary commuting features and the automated vehicular feature will constitute the majority of the percentile rank of motor automobiles just in the business sector by 2020 [1]. The establishment of a smart automotive sector may indeed cause moral indignation, the stress distribution of vehicle riding, and tackle the issues of environmental depletion of natural resources induced by transportation jams.

The automated recognition of cycle lanes just on the roadway is indeed the technological underpinning for automobile-aided navigation as well as an essential piece of such theory was developed in autonomous cars [2]. Somewhere at the moment, the major mechanisms of traffic signs used domestically and overseas are as follows: the technique of recovering route characteristics using computer vision technology, the way of constructing a roadway design for recognition, and indeed the technique of multi-sensor fusing sensing [3]. As the number of cars on the road has grown throughout the years, so has the number of casualties. It kind of endangers people's well-being but also generates massive financial damages. Unless a computer network can indeed be utilized to observe the immediate data in real-time while operating and detect potential hazards as soon as feasible, traveling efficiency might be considerably enhanced. Traffic monitoring, like that of the foundation and basic function of autonomous navigation systems, has piqued the interest of academics.

Automobile recognition is particularly critical at dark when the illumination and clarity are low and indeed the likelihood of a vehicle crash is greater. There are two kinds of important transport recognition strategies: those associated with classical image retrieval and those based on deep neural networks.

Conventional object recognition systems employ low-grade characteristics for edge detection [1], notably automobile offers breath taking at night time. Hsia detected the lane markings using the Hough transform, and then after acquiring the led source information for every track, the automobile number was calculated based on the viewing angle as well as dispersion of the background light [2]. Jong provided an enhanced multi-scale retina (MSR) contrast augmentation technique, and a two-stage predictor relying on BoF and CNN was employed to eliminate false alarms [3]. In the above dark automobile recognition approach is directly persuaded by roadway sceneries because it is reliant on automobile beam attributes and algorithms. As a result, it is dependent on human background subtraction.

Overview:

Machine learning algorithms have indeed been extensively employed in a variety of sectors in the world, particularly machine learning, automated vehicles, and networking site applications. The advancement of detectors including GPUs, as well as artificial neural networks, has expedited the exploration of machine life driverless driving. To provide secure as well as precise critical thought, a driverless car having self-driving capacity should reliably recognize automobiles, passengers, road signs, streetlights, and so forth instantaneously. Photonics, Light Detection and Ranging (Lidar), as well as Radio Detection and Range (Radar) devices, are commonly employed in self-driving cars to identify these things. An optical system, between many measuring instruments, could effectively detect the displaying content depending on the surface plus tone attributes but is far more expensive than some other detectors. Deep learning-based item identification utilizing image devices, in particular, has become more relevant in driverless automobiles since it reaches an improved prediction performance over humans when it comes to image classification, making it a crucial tool in driver assistance technologies. The two additional steps must be followed by an automated method for self-driving cars. Initially and foremost, a great recognition rate of street items is essential. Secondly, actual recognition performance is critical for such an automobile operator's quick reaction plus low delay.

Deep learning-based item classification methods, which seem to be essential in self-driving cars, are divided into two types: two-stage sensors and one-stage sensors. Fast R-CNN, Faster R-CNN, and RFCN are two-stage sensors that perform the first step of fully connected creation, followed by the second stage of object categorization and box regression. Such approaches, while typically accurate, have had the drawback of a sluggish classification performance with poor productivity. Entity categorization plus box regression are performed simultaneously by one-stage sensors, such as SSD as well as YOLO, in the absence of an area planning phase. Such approaches offer good recognition effectiveness and quality, and yet a poor performance. Entity sensors integrating diverse techniques have indeed been intensively investigated in current times to make use of various methodological approaches and adjust to their drawbacks. MSCNN, a two-stage sensor, increases recognition rate by detecting several intermediary neural levels. SINet, a two-stage sensor as well, offers quick recognition by utilizing a spectrum system. To boost the recognition rate, CFENet, a one-stage sensor, employs a complete information augmentation higher unit on SSD. refined, a one-stage sensor as well enhances recognition rate by combining an attachment modification component as well as an image recognition component. RFBNet, this other sensor, uses a visual cortex barrier to reduce errors. Nevertheless, prior research failed to satisfy an actual recognition rate of over 30 fps, which also is a necessity for self-driving systems, while employing an intake scale of 512 512 or more, which would be typically used in object identification algorithms for obtaining good precision. Although actual recognition is feasible, the poor precision makes it challenging to use driverless cars. This suggests that perhaps the prior techniques are lacking in regards to an exchange among precision and productivity is affected, and as a result, its applicability to self-driving devices is limited. Furthermore, amongst the most serious issues with many traditional deep-learning-based entity recognition methods would be that, while the box dimensions (i.e., recognition and tracking) of such identified items are available, the ambiguity of a box outcome isn't really. As a consequence, traditional entity sensors (i.e., FPs) could avoid mislocalizations since they simply report the predictable findings of a box devoid of any data about the ambiguity. An FP represents an erroneous classification performance of a box on an item other than the ground truth (GT), or perhaps an erroneous recognition outcome of the box upon that GT, although a TP indicates a precise measurement outcome of the box upon that GT. With driverless cars, an FP is particularly risky since it produces inappropriate reflexes such as abrupt brakes, which might diminish safety.

In various terms, it really is critical to forecast the ambiguity of such identified boxes as well as to take this element into account, including the objectness rating but also category ratings, in order to reduce the FP and thus minimize self-driving mishaps. As a result, several pieces of research on anticipating risk in pattern recognition have indeed been done. Kendall et al. suggested a computational intelligence estimation approach for risk assumption based on a Bayesian deep net. Feng et al. suggested a technique for estimating ambiguity based on Kendall et al. methodologies applied to 3D automobile identification with a Lidar sensor. The approaches provided by Kendall et al. as well as Feng et al., on the other hand, simply estimate the amount of ambiguity but do never use it in real implementations. Choi et al. presented and implemented a technique for estimating ambiguity instantaneously that used a Gaussian combination theory in a self-driving scenario. Nevertheless, it must have been used to drive direction rather than entity recognition, and then as a result, a sophisticated dispersion is represented, adding computing difficulty. He et al. devised as well as used a method for anticipating variance to entity recognition. Yet, since researchers concentrated on such a two-stage sensor, their technique could not handle real-time functioning and still suffers from a box overflow issue, reducing the availability for self-driving purposes. To address the shortcomings of prior image recognition investigations, this work offers a unique entity recognition technique relying on YOLOv3. YOLOv3 may identify several entities with such a given assumption, which increases the recognition rate; moreover, by employing a non-linear and non-recognition approach, this could compensate for such high error of YOLO or YOLOv2. Depending on such benefits, YOLOv3 is appropriate for driver assistance purposes, although yields lesser precision compared to a two-stage technique. As a result, it's indeed critical to enhancing precision whilst keeping actual image detecting capabilities.

To that end, the current research presents a strategy for enhancing the recognition rate through characterizing the box dimensions of YOLOv3, which only really produces predictable data, as Gaussian variables (i.e., average plus variation), as well as revising the box gradient descent. A clustering risk for a box regression job in YOLOv3 may be evaluated using Gaussian simulation. Moreover, a strategy for minimizing the FP and boosting the TP using exploiting the expected clustering ambiguity of said box throughout the identification phase is presented to increase the recognition rate even faster. As a result, this is the earliest approach to describe the clustering ambiguity in YOLOv3 including using this element in such a realistic circumstance.

As a consequence, the suggested Gaussian YOLOv3 could handle mislocalizations in self-driving scenarios. Furthermore, since this suggested technique would only be loosely based within box of such YOLOv3, qualitative data was obtained (in other words, the activation function), the additional computation value is irrelevant, as well as the suggested methodology retains the actual recognition rate of above 42 fps with just an informal settlement of 512 x 512 given the substantially improved efficiency. Mostly on KITTI and BDD datasets, the suggested Gaussian YOLOv3 enhances the mAP by 3.09 and 3.5, correspondingly, relative to the prediction model (i.e., YOLOv3). Furthermore, also on KITTI plus BDD collections, the suggested technique decreases the FP significantly by 41.40% and 40.62%, correspondingly, while increasing the TP by 7.26 percent but also 4.3 percent, in both. As a consequence, in respect of the exchange among precision as well as affected productivity, the suggested method is appropriate for driverless vehicles since it enhances recognition rate and tackles the mislocalization issue whilst allowing authentic functioning.

Even as the number of cars on the road has grown in previous times, so has the number of road mishaps. This not only endangers individuals' safety and moreover generates massive financial damages. When a computerized technology could be utilized to observe the immediate data in real-time while riding and detect potential hazards as soon as feasible, vehicle security might be considerably enhanced.

Object tracking, as even the foundation key basic job of autonomous navigation systems, has piqued the interest of academics. Automobile recognition is particularly critical at dusk, when the light plus clarity are low as well as the likelihood of a speed collision is greater. There are two kinds of important transport recognition methodologies: those relying on classical image retrieval and those focused on deep neural networks. Conventional traffic surveillance systems employ low-level characteristics for image retrieval, particularly automobile luminous data at twilight. Hsia detected the lane dividers using the Hough transform, and then after acquiring the brightness collected information for every track, the automobile quantity was calculated based on the viewing angle and separation of said beam of light. Jong developed a better multi-scale retina (MSR) contrast augmentation technique, as well as a two-stage predictor built on BoF with CNN to decrease misclassification. As shown above, nocturnal automobile recognition approach is directly persuaded by roadway sceneries because it is reliant on automobile lighting attributes and algorithms.

As a result, it is dependent on human image retrieval. Machine learning technology created a new realm for source localization as well as dramatically enhanced goal recognition results. Traffic monitoring employs Faster-RCNN, YOLO, SSD, and some similar vision-based algorithms. Wang tested the performance of machine learning in automobile recognition using five fully convolutional vision-based algorithms mostly on the KITTI sample. By enhancing the routing path of YOLOv2, He et coupled it with a millimeter-wave laser to determine the location of an automobile but also accomplished quick identification of vehicle threats. This decreased the detection period even more. Nevertheless, such methods do a massive proportion of computation and therefore demand sophisticated equipment to function. As a result, M-YOLO was suggested in this report. It is appropriate for usage in restricted locations, such as integrated electronics in cars. Furthermore, it does have a greater recognition accuracy.

Project Description:

A lane sensor network relying on enhanced Yolo v3 method is described to address the concerns of high error with poor authentic efficiency of the Yolo v3 method in target tracking. To begin, lane line images are separated into s * 2S grids based on the features of uneven transverse and longitudinal dispersion frequency. Furthermore, the sensor range has been reduced to four observation levels, making it more suited for tiny object identification, like lane line detection. Thirdly, to reduce the system, the CNN model within the initial Yolo v3 method is reduced from 53 to 49 levels. Lastly, characteristics like cluster center range and transfer functions are enhanced. According to the testing data, while utilizing the enhanced recognition system for lane line recognition, the accurate sensing error map number is 92.03 percent as well as the response time is 48 frames per second. It outperforms the classic Yolo v3 methods in terms of efficiency rate and authentic speed.

1.1 Problem Definition

Today there is a lot of research on ADAS (Advanced Driving Assistance System) where everything from" Lane Departure Warning (LDW)" to" Full autonomous driving" is investigated. However, there is a need for research about the integration of safety critical applications and non-safety critical applications on a mixed criticality platform where the two applications are isolated

from each other using virtualization. For example, Autoharp, which is a partnership for development of software founded by major players in the automotive industry, does address mixed criticality systems in the sense that they recognize that the standards must be supported on their platforms. This thesis will investigate different techniques for road and lane detection and how they can be implemented on the real-time operating system (RTOS) of a Mixed Criticality System. YOLO identifies entities by partitioning a picture using matrix cells, as opposed to a fully connected approach used throughout two-stage sensors. The YOLO production element's characteristic mapping is a technique to report box dimensions, the entity categories value, as well as the category values, allowing YOLO to recognize many entities with such a given prediction. As a result, the recognition rate is way more efficient than among traditional approaches. Yet, because of each matrix command's computation, positioning inaccuracies are considerable and the recognition rate is poor, reducing the availability for driver assistance purposes. YOLOv2 has indeed been presented as a solution to such issues. When opposed to YOLO, YOLOv2 enhances recognition rate by adding phase normalization for such tensor operation, as well as an attachment box, inter learning, plus perfectly alright characteristics. Nevertheless, for tiny or thick particles, the recognition rate remains inadequate. As a result, YOLOv2 is inappropriate for driver assistance systems that demand great precision for numerous roadway elements and tiny items like road signs with signals. To address the shortcomings of YOLOv2, YOLOv3 has already been suggested. YOLOv3 is made up of fully connected layers as well as a neural structure for excellent precision, as seen in Figure 1a. YOLOv3 solves the degradation issue of convolutional models with a leftover experience or association as well as a slightly higher compared plus splicing strategy that retains perfectly alright characteristics for tiny item recognition. The much more noticeable characteristic is recognition at three separate sizes, comparable to how a multilayer perceptron system works. This enables YOLOv3 to locate anomalies of varying dimensions. In a greater context, when such imagery with three components of R, G, plus B is fed through the YOLOv3 model, as illustrated in Figure 1a, image recognition data (box coordinates, objectless rating, but also category ratings) is produced through three detection levels. The projected findings of a three-sensor level are pooled then the non-maximum reduction is used to analyze them. The features extraction findings are then calculated. Since YOLOv3 is a deep convolutional system composed exclusively of comparatively tiny inversion files of 1 x 1 and 3 x 3 resembling YOLOv2, its prevention activities are comparable to that of YOLO and YOLOv2.

As a result, YOLOv3 is suited for self-driving implementations and thus is frequently employed in driver assistance studies due to the exchange between precision and reliability. Consequently, it does have a poorer overall efficiency when compared to a two-stage sensor with an area planning phase. The Gaussian analysis but also transfer functions rebuilding of YOLOv3 suggested in this study could be similarly comparative by lowering the effect of imbalanced datasets throughout retraining and forecasting clustering risk. Furthermore, employing this anticipated clustering ambiguity could improve the recognition rate yet higher.

1.2 Project Overview/ Requirement Specifications

1.2.1 Introduction

It is critical for a driverless car to identify items in its surroundings in order to function properly. This report discusses how to identify and analyze things to aid driverless cars. Among the most significant conditions for driver assistance systems in driverless cars is the duty of image classification. Deep learning, several of the machine learning jobs, performs image classification much more successfully than previous approaches, and indeed the scope of this study is to recognize items such as automobiles, people, traffic signals, and so forth. Throughout this report, we look at a deep learning technique to entity recognition that predicts the bounding box of an appearance. The process of recognizing things in an input dataset is known as image classification.

1.2.2 Input

Vehicle, Image, Driverless, Lane

The system should be completely configured before the usage, and even the consumer has to be familiar with relevant structure. Whenever the construction is ready, you must save it prior to departing so that the core may be piled for future use. The standard has indeed been raised.

1.2.3 Processing/Flowchart

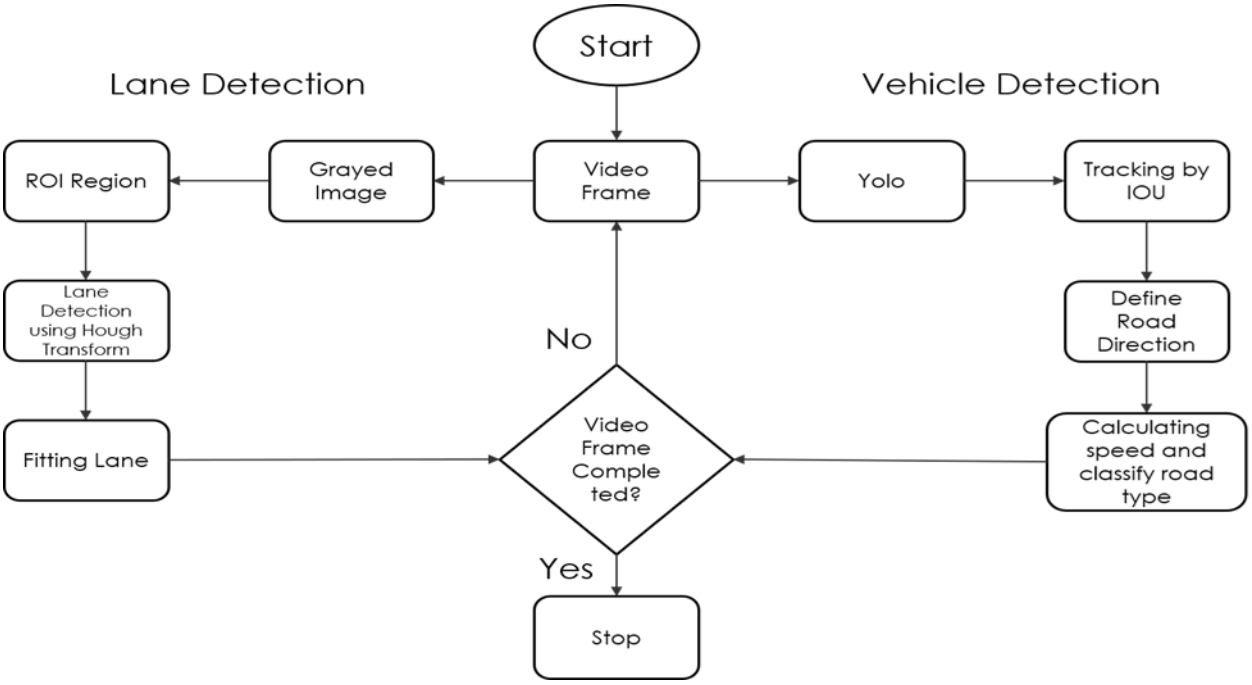

Figure 1 Flowchart

1.3 Hardware Specifications

Minimum Requirements	**Windows**
Operating System	Windows 7
Processor	Dual core, Intel i3
RAM	2 GB RAM
DISK Space	The amount of disc space available depends on the partition size and whether or not online help files are allowed. The Math Works installer would tell you how much disc volume your partition needs.

Graphics Adapter	8-bit graphics adapter and display (for 256 simultaneous colors)
CD_ROM drive	For installation from CD

Recommended Requirements	**Windows**			
	Processor	**RAM**	**DISK Space**	**Graphics Adapter**
PYCHARM-Python IDE	Intel i3	2 GB	1 GB for Pycharm only. 5 GB for a typical installation	A 32-bit or 64-bit OpenGL capable graphics adapter is strongly recommended

1.4 Software Specifications

Tensorflow
YOLOV3
Numpy
OpenCV 3
Pandas

Language

- Python
- Numpy
- OpenCV
- Pandas
- Tensor Flow
- Yolov3

Chapter 2: LITERATURE SURVEY

2.1 Proposed System

2.1.1 Summary of the LaneRTD Algorithm

The LaneRTD approach has the benefit of just using just a solitary Imaging system. To record the whole front driver's view, these lenses must be positioned mostly on the vehicle's front-windshield reflector. Besides presuming that perhaps the standard is sufficiently level, the skyline is guaranteed to just be aligned towards the X-axis mostly in the snapshot. Nevertheless, if indeed the skyline is indeed not aligned to that same X-axis, then the device's measurement information might be analyzed to correct the alignment. To be clear, the road borders are typically organized in sets of markers that are often square in shape (or approximate). LaneRTD (Lane Real-Time Detection) seems to be another sort of technique stated [5]. The usage of this method in real life is indeed a benefit. The key operation of this technique is the reduction of signal-to-noise ratio as well as the recognition of vehicle channels' borders using Canny edge identification [6]. Canny detecting sides enable others to delete borders that do not "please" them in order to achieve the maximum representation of the shape of such seen item. It really is mainly used on black-and-white photos with such a Gaussian filter added [7], which enables them to eliminate clutter. It really is vital to note that now the Hough transformation [8] is used to identify the locations of something like the driving lane, although, from the dynamic array results, it is feasible to show the car lane just on video sequence using a few more techniques. This project is focused here on the form of channel identification and tracking. Specific parameters have such a three-channel memory. As shown in Figure 2, H, S, V, and H, S, L indicate the color tone, S color immersion, V color depth, and L color brightness. Furthermore, several other color intensity schemes, including such HSV (Hue, Saturation, Value) as well as HSL (Hue, Saturation, Value) Saturation, Crispness, could be stated to produce the lane of traffic whatever is easier identified using incoming films. Filters have such a three-channel memory. As shown in Figure 2, H, S, V as well as H, S, L indicate the shades, S color saturation, V color change, and L color luminosity. When employing such places, you may come into the need to define a barrier so that roadways are more protected and feasible. Specific parameters have such a three-channel memory. As shown in Figure 2, H, S, V, and H, S, L indicate the color tone, S color immersion, V color depth, and L color brightness.

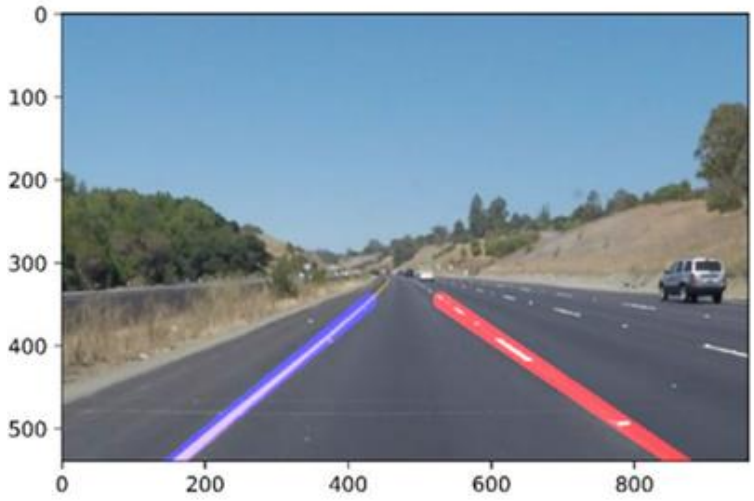

Figure 2 Detected Lane boundaries by the LaneRTD algorithm

Furthermore, several other color intensity schemes, including such HSV (Hue, Saturation, Value) as well as HSL (Hue, Saturation, Value) Saturation, Crispness, could be stated to produce the lane of traffic whatever is easier identified using incoming films. Filters have such a three-channel memory. As shown in Figure 2, H, S, V as well as H, S, L indicate the shades, S color saturation, V color change, and L color luminosity. When employing such places, you may come into the need to define a barrier so that roadways are more protected and feasible

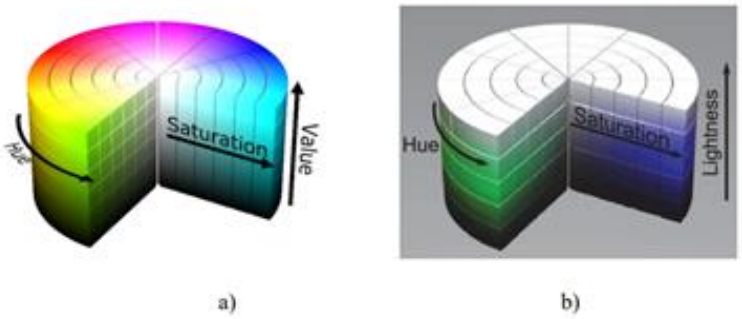

Figure 3 Color space [9]: a) HSV1, b) HSL2

2.1.2 CANNY EDGE DETECTOR

The standard Canny algorithm's basic stage is to flatten the picture. Canny calculated the whole first gradient of the Gaussian filter, which would be the closest approach to the ideal feature extraction activator. Select a suitable 1-d Gaussian filter to flatten the picture based mostly on the sequence as well as the panel, i.e., apply compression upon this digital image. Because the Fourier process obeys both distributive and algebraic laws, the Canny technique often employs a two-dimensional Gaussian filter (as illustrated in (1)) to flatten the picture and reduce outliers.

$G(x, y) = exp[-(x2 + y2)/2\sigma 2]/2\pi\sigma 2$ ------- (1)

where σ is the Gauss filtration system variable that regulates the extent of picture softening. The amplitude and phase of the picture slope are calculated in the second phase. To evaluate the cost and orientation of pixel intensity, the classic Canny technique uses a restricted variety of 22 surrounding communities [9]. The accompanying formulae could be used to calculate the very first-degree fractional derivative's estimate in the X and Y-axis:

$Ex[i, j] = (I[i + 1, j] - I[i, j] + I[i + 1, j + 1] - I[i, j + 1])/2$ ---- (2)

$Ey[i, j] = (I[i, j + 1] - I[i, j] + I[i + 1, j + 1] - I[i + 1, j])/2$ ----- (3)

As a result, the picture gradients computation driver's template are:

$GX = \begin{matrix} -1 & 1 \\ -1 & 1 \end{matrix}$ ---------- (4)

$Gy = \begin{pmatrix} 1 & 1 \\ -1 & -1 \end{pmatrix}$ ---------- (5)

Scale and direction of the inclination may be calculated. Image on a gradient scale is:

||M(i,j)||=√([[E_x [i,j]]]^2+[[E_y [i,j]]]^2) (6)

The azimuth of the picture slope is:

$(i, j) = arctan(Ey[i, j]/\ Ex[i, j])$ ---------- (7)

The Canny edge detector [8] works by calculating the slope of the image twice. Sides are therefore determined as feature points of the mean vector that are greater than certain criteria. Non-maximum suppression, or NMS, is the name given to this threshold highest qualities classification algorithm. The goal behind Canny's edge generator would have been to create an "ideal" activator within view that minimizes the likelihood of repeatedly identifying a line, the chance of refusing to accept a border, and the gap between the claimed side as well as the genuine corner. The very first two of all these requirements fix the challenges of recognition, that is, would the segmentation method locate an area if one exists? (and no other edges). The third component tackles the problem of navigation, or how correctly a side's location is conveyed. There is indeed an exchange among detection and recognition: the better the sensor, the worse the localization, and likewise.

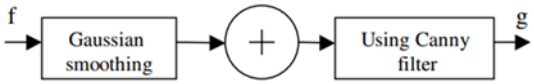

Figure 4 Block diagram of image enhancement (sharpening and de-noising) using Canny edge detector

The Canny technique may recognize body boundaries in pictures. This technique could potentially identify a cloud's border. John F. Canny created the Canny activator in 1986, which used an inter broad range technique for picture aspect identification. John F. Canny explored but also resolved the statistical challenge of determining which screen is by far the best effective depending on sensing parameters including minimal localization or receiving many replies for just a dedicated line. The method is divided into five categories: (1) smear; (2) brightness differential detection; (3) non-maximum reduction; (4) dual cutoff screening; and (5) loop median filter. By precisely identifying the border slopes of such components, the Canny sensor responds towards the genuine borders of such a picture and therefore is resilient to fake margins. It moreover responds to such curvature just once, removing the influence of vast illumination fluctuation regions just on corners. The Canny method is sensitive to interference. The Gaussian haze is such a method for reducing the impression of uncertainty on a picture. It is a visual fading method that uses a Gauss unit (3 x 3, 5 x 5, 7 x 7, etc.). Each cell's size is determined by the required amount of picture distortion. The haze impact is much less evident when the cell's size is lower

2.1.3 HOUGH TRANSFORM

The Hough transform is well acknowledged as a strong pattern analysis tool that produces reasonable outcomes often in the face of distortion and diffraction. The method's main disadvantages are its high material needs and computation cost. Illingworth and Kittler (Comput. Vision Graphics Image Process.44, 1988, 87-116) provides a very thorough assessment of known approaches up to and beyond 1988. The present project offers information on cutting-edge Hough approaches. This comprises analysis and comparison of current approaches, recent conceptual viewpoints, a large number of original methods, concurrent applications, and enhancements to mission equipment. It is important to make the distinction between work that tries to advance basic knowledge of the studies but is not always feasible and development that could be relevant in an industry situation. The Hough transform is a technique for recognizing contours in a color or monochrome picture. This technique enables you to provide required specifications for curvature segments but also guarantees that the predetermined subset of curvature is detected in the picture. Shapes of many forms, including horizontal planes, spirals, and rounds, could be identified. This even supports recognition depending upon a pre-set pattern. To discover the curvature subgroup, the Hough transform method employs an aggregate field, the size of the image among which gives the degree of uncertain variables in the calculation. While recognizing the curvature y = m*x + b, for instance, all readings for such variables m and b for every column should be determined. Throughout this example, the data are aggregated within component matrix A [M, B] thus reflecting the likelihood of the presence of columns according to the formula y = m*x + b within the studied imagery, where M and B are distinct quantities of m and b. The Hough transformation is performed in climatology but also hydrologic.

2.1.4 THE KALMAN FILTER

To use a sequence of data made over a period, the Kalman filter calculates a likelihood function across the parameters of such an entity within consideration. This enables for a reduction mostly in the influence of disturbance on the variable during the examination as well as reduced inaccurate data throughout the prior, current, and beyond. The Kalman filter is a cyclical limiter that performs an ideal evaluation of a brief condition of a continuous stochastic process which is impacted by the Gaussian filter with such a standard deviation based on the observations acquired. The Kalman filter is primarily used to evaluate the procedure involved in x R, in which the system is represented by regular nonlinear equations (vector and matrix forms).

2.1.5 YOLO ARCHITECTURE

The purpose of this study is to investigate a much more appropriate detecting method for usage mostly in car's integrated platform. The ultralight connection Mobilenet v2 was chosen as that of the communications system for image retrieval in the suggested M-YOLO. Mobilenet v2 may considerably minimize the model's variables plus computations, as well as increase the model's system efficiency. The sensor unit continues to employ the YOLO v3 inter forecasting component. The EIoU error rate is used to optimise the gradient descent. Furthermore, for such sample in just this paper, the k-means technique is utilized to re-cluster as well as obtain Appropriate bounding box. Figure 4 depicts the M-YOLO suggested framework described in this report.

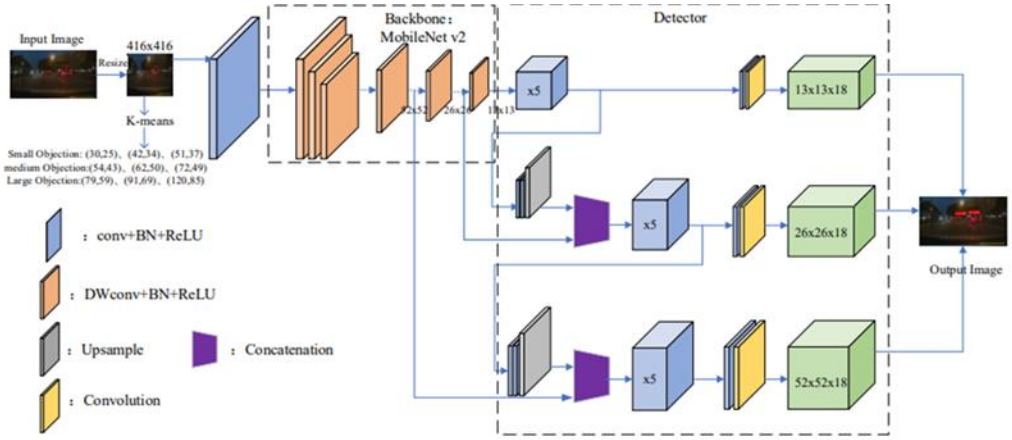

Figure 5 Network structure diagram of M-YOLO 2.1.

2.1.6 YOLO (You Only Look Once)

1. Residual blocks

- Initially, the image is subdivided up into various grids. Each grid is S × S in size. How a grid is created from a source image is shown in the below diagram

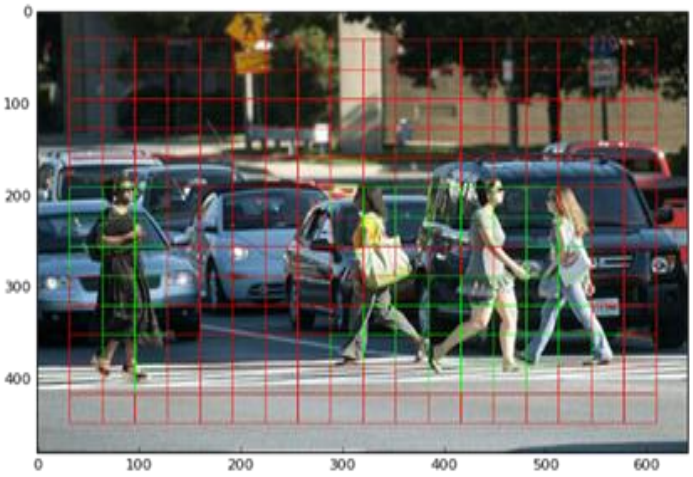

Figure 6 Residual Blocks

- Several grid cells of the same size are given in the image above. Each grid cell detects Objects that occur within the grid cells. If an item center arrives within a certain grid cell, for example, that cell will be responsible for detecting it

2. Bounding box regression

- An outline in a photo that draws attention to a certain object is called a bounding box.
- It has the following attributes:
    1. Width (bw)
    2. Height (bh)
    3. Class (for Ex, person, car, traffic light, etc.)- This is represented by the letter c.
    4. Bounding box centre (bx, by)
- A bounding box represents an object's height, width, centroid size, and class. To determine its height, width, and class, YOLO uses a single regression.

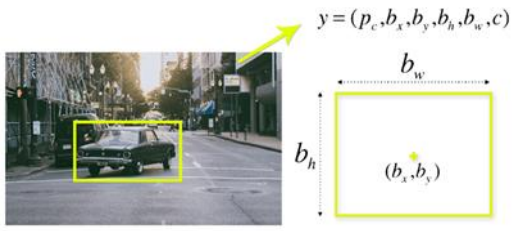

Figure 7 Bounding Box Regression

- To determine the height, breadth, and class of objects, the YOLO algorithm involves a single bounding box regression.
- The intersection over union (IOU) technique shows how object detection is done by overlapping boxes. IOU is implemented in YOLO to generate an output box that correctly surrounds the objects.

UBBR accepts not just images and moreover (approximately localized) boxes which will be altered to closely surround neighboring items. As a result, every type of technique must be presented alongside such boxes. Moreover, the boxes given to a layer are connected ought to be various in order for UBBR to really be ubiquitous, but they must also coincide including at minimum single ground-truth to a certain level such that UBBR could notice sufficient proofs regarding the objective item. To that purpose, we construct source bounding boxes during retraining by randomizing modifications to ground-truth boxes. Let $g = [xg, yg, wg, hg]T$ constitute a ground-truth box represented with its core organize (xg, yg), width wg, and height hg. Conversion factors for all four values that are included in the sample from the single deployments independent in the following manner:

$$tx \sim U(-\alpha, \alpha)$$
$$ty \sim U(-\alpha, \alpha)$$
$$tw \sim U(ln\,1 - \beta, ln\,1 + \beta)$$
$$th \sim U(ln\,1 - \beta, ln\,1 + \beta) \quad (1)$$

Then one fortuitous input box b = [xb, yb, wb, hb] > is derived by employing the sampled conversion to g:

$$Xb = xg + tx \cdot wg$$
$$Yb = yg + ty \cdot hg$$
$$Wb = wg \cdot exp(tw)$$
$$Hb = hg \cdot exp(th) \quad (2)$$

Furthermore, if the IoU across b and g is smaller than even a predetermined limit t, then merely reject b throughout learning. Experimental values for α, β, and t are 0.35 and 0.5, correspondingly. Figure 5 depicts several arbitrary box generation instances.

Figure 8 *Example of randomly generated bounding boxes for training UBBR. Black boxes are ground-truths and yellow ones are randomly generated boxes.*

3. Intersection Over Union (IOU)

- In each grid cell the bounding boxes and their confidence ratings are forecasted. The IOU is 1, when the predicted and actual border boxes are identical, the IOU is 1. To remove bounding boxes that are not the same size as the main box this approach is used.
- A simple illustration of how an IOU works is shown below.
- The image below describes two bounding boxes, one in green and one in blue. The blue box represents the anticipated gift, whereas the green box represents the actual box. YOLO guarantees that the size of the two border boxes is the same.

IOU (Intersection over Union) is a phrase intended to define the amount to which two boxes intersect. The bigger the crossover zone, the bigger the IOU. IOU is mostly utilized in image object tracking, wherein they build a system to estimate a box which matches completely over an item. The goal of this process would have been to continually refine its forecast till the both boxes completely coincide, i.e., the IOU between both the two boxes equals one. IOU is indeed employed in non-maximal suppression. IOU can also be implemented in non-maximal repression, that would be intended to remove numerous boxes which enclose similar object according to which box will have the most certainty.

4. BOUNDING BOX REGRESSION

These area suggestion methods (for example, Selective Search) evaluate an initial picture to determine the location of a prospective entity. Worth noting that they also have zero clue if such a result is found in a certain spot; all they know would be that the region of the images appears intriguing and demands additional investigation. These area suggestions were utilized within basic version of Girshick et al's R-CNN, to retrieve yield attributes from such a pre-trained CNN (without the fully-connected level leader) and afterwards passed into such an SVM for validation set. The site from either the local offer was used as the bounding box throughout this approach, and the SVM generated the classification model for such bounding box area.

Basically, the initial R-CNN model could not "understand" what to do to identify bounding boxes – it would not be capable of learning from edge to edge (future iterations, such as Faster R-CNN, actually were end-to-end trainable).

However, this poses the following concerns:

• What about if one wished to develop an end-to-end feature selection method?

• Could it be necessary to form a classifier model that could produce bounding box dimensions, allowing us to retrain the method to generate good accuracy of entity detectors?

• But, assuming that's the case, then do we have to go regarding learning what a framework is?

5. LOSS FUNCTION

The deep convolutional neural network's deficit formula is performed to determine the gap between the expected as well as actual values. YOLO v3's error rate is mostly made up of locality reduction, optimism failure, plus category failure. Category reduction plus conviction reduction in M-loss YOLO's mechanism are much the same as YOLO v3. However, the localization reduction employed EIoU decline.

YOLO v3's mobility degradation employs the root means square loss function (MSE) calculating the Euclidean distance. The IoU logistic regression, when contrasted to Euclidean distance, might adequately define the crossover between both the estimated and actual thresholding. As a result, YOLO employs the EIoU gradient descent, which accurately reflects the shape and size of the enclosing box.

The total loss function of M_YOLO is as follows:

$$Ltotal = Lbox + Lconf + Lclass$$

IoU deficits are being used for extrapolation requirement rather than usual ones like L2 plus flat L1 costs. The disadvantage of typical bounding box regression costs would be that the bounding box modification variables ((tx, ty, tw, th) are optimised separately, despite the reality that they will be strongly cross - functional. IoU damage has indeed been suggested to resolve this challenge, since we found that even when contrasted to flat L1 reduction, IoU decline enables for much more steady learning and results to superior results. For convergence time, simply add a minor variable £ to the IoU figure while performing the logarithmic. The mean of said box-wise analysis errors would then be described as even the image-level damage:

wherein bn would be an inputs box while gn seems to be the ground-truth bounding box which optimally overlaps with bn according to the IoU measurement. In addition, UBBR(bn) represents the alignments anticipated by UBBR, and f represents the hough transform which optimizes bn with said projected mitigate values.

6. Merge of the 3 techniques

- The below image shows a combination of three methodologies to produce the last detection result.
- To split the picture Grid cells are used. In every grid cell, B bounding boxes are projected, along with their reliability or best output score. The class probability of the cell is estimated to identify each item class.
- At least three various types of objects are identified, including a truck, a dog, and a bicycle.

To construct all of the projections at the same time A single convolutional neural network is used. When IOU is utilized, the object's bounding box boxes are just like the object's actual boxes. This phenomenon eliminates any unnecessary bounding boxes that do not correspond to the attributes of the items (like height and width). The end detection will consist of separate bounding boxes that are tailored to the objects.

2.2 Detection of clouds and ground surface based on the color

It is feasible to distinguish between images that correspond to clouds as well as images that correspond to the atmosphere itself by analyzing the proportion between both the red and blue bands. As per Long et al., mists do indeed have a significant color equilibrium proportion. A study of the mean earnings of hues enables the separation of storms out from the ground atmosphere. Complicated boundary recognition techniques, such as those examined in the paper, might be applied. Yet, it is reported that all these methods take between 0.3 and 61.1 seconds to operate on 1024 x 768 quality panel pictures. This boundary recognition rate is quite sluggish, particularly because it is rarely essential to identify the boundary quite precisely whenever the processing efforts may be efficiently employed for detecting cumuliform clouds. A hypothesis may be established that comparing other color proportions enables identifying the skyline in less than 0.3 s or deleting the border by just discarding the bottom portion of the image.

2.3 Description of the suggested Hough Transform & Canny Edge Detector based cumuliform cloud detection method

As said before, because the pattern of chaotic complexity clouds is modified by circulation, the implementation of the Hough transforms in principle might enable detecting the locations containing chaotic complexity clouds mostly in photos. To use the Hough transform, the picture must be altered such that somehow the borders of the entities remain. For such an objective, the Canny method is utilized. Throughout the research, the OpenCV package got employed. In general, the cloud recognition technique comprises of first analyzing the picture with the Canny technique, then applying the Hough transform to calculate the independently identified sections plus dots. The screen was turned into a 4×4 matrix form with 16 quadrants over the research.

The calculation of arcs plus squares is done independently for every sector of a screen, rather than for the entire structure. Because the number of identified squares and curves varies by sector, the Kalman filter is employed separately in every region by normalizing the frequency of recognized squares and curves. A cutoff value was used in the last step to assess whether the similarity between these two squares and curves in a sector exceeded a speed regulation. If indeed the limited processing yields a high value, the sector is assigned to a chaotic complexity atmosphere. It is indeed feasible to estimate the proximity of a cloud. Nearby clouds would be discovered just at

peak of the frame if indeed the lens is below that of the cloud bottom, however, clouds afar distant would be seen inside the bottom segment. In just this example, the upper regions will just have nearer clouds, while the bottom regions towards the skyline would have had clouds farther off. Using all these principles, a program was developed to detect chaotic complexity clouds amid one backdrop of space or even other clouds. Figure 6 depicts the algorithm's flow diagram.

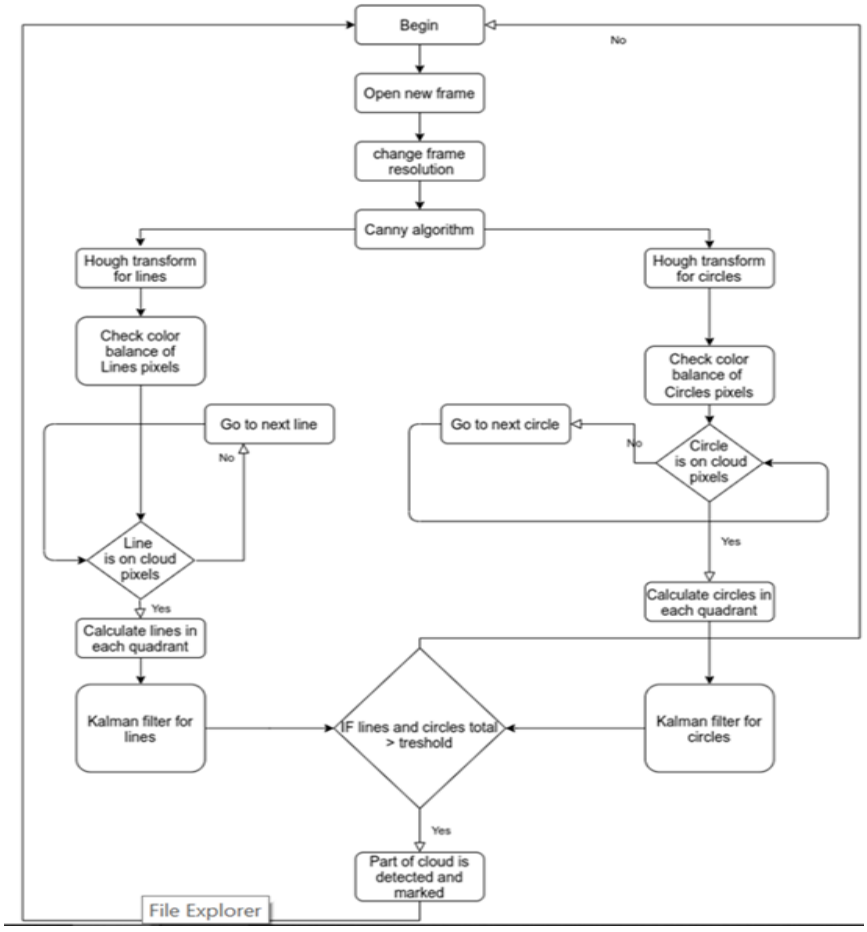

Figure 9 Diagram of the proposed algorithm

2.4 GAUSSIAN YOLOv3

The predictive characteristic mapping of YOLOv3 comprises three forecast boxes for each panel, as seen in Figure 7, with every prognosis box consisting of box dimensions (i.e., tx, ty, tw, and th), the objectness value, and subclass values. YOLOv3 returns a value from zero and another for objectness (if a cell contains or not from the box) plus subclass (the categorization of the item). The combination of such two numbers is subsequently used to identify an item.

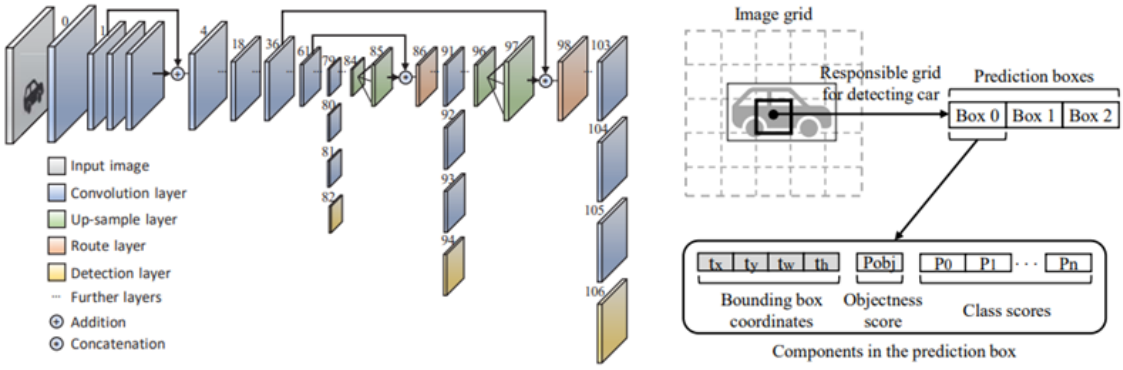

Figure 10 Network architecture of YOLOv3 and (b) attributes of its prediction feature map.

Box dimensions, despite objectless but also category data, are presented as predictable bounding boxes rather than a grade, hence the certainty of the discovered box is uncertain. Furthermore, the objectness rating somehow doesn't properly represent the box's dependability. As a consequence, it has no idea how unpredictable the outcome of the box is. On the contrary, the suggested product's prediction of box instability acts as the box scores and may therefore be utilized as a measure of how unpredictable the box is.

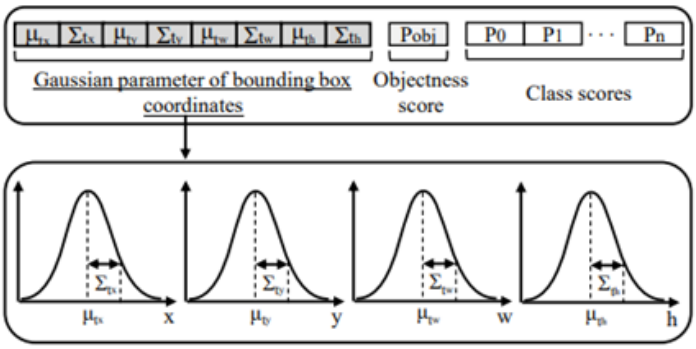

Figure 11 Components in the prediction box of the proposed algorithm.

Box regression is used in YOLOv3 to retrieve box center data (i.e., tx and ty) as well as box dimension data (i.e., tw and th). The complicated analysis is indeed not necessary to estimate the clustering ambiguity since there is a unique right response (i.e., the GT) given an entity's box. In alternative terms, any Gaussian model of tx, ty, tw, and th. may be used to represent the ambiguity of the box. A solitary Gaussian version of predicted value y with Gaussian variables for just a testing set input x is as described in the following:

$$p(y|x) = N(y; \mu(x), \sum(y)) \quad (1)$$

where μ(x) and Σ(x) are among the average and dispersion features, respectively. Forecasting ambiguity of box, for each of the box aligns in the calculation trait map is shaped like the mean (μ) and variance (Σ), as shown in Figure 2. The end product of box are μˆtx, Σˆ tx, μˆty, Σˆ ty, μˆtw, Σˆ tw, μˆth, and Σˆ th. Take into account, the composition of the recognition level in YOLOv3, the Gaussian constraints for tx, ty, tw, and th are pre-treated in the following manner:

$$\mu tx = \sigma(\hat{}\mu tx), \mu ty = \sigma(\hat{}\mu ty), \mu tw = \hat{}\mu tw, \mu th = \hat{}\mu th \quad (2)$$

$$\sum tx = \sigma(\sum\hat{}tx), \sum ty = \sigma(\sum\hat{}ty), \sum tw = \sum\hat{}tw, \sum th = \sum\hat{}th \quad (3)$$

$$\sigma(x) = 1/(1 + exp(-x)) \quad (4)$$

The anticipated vector of the box is represented by the average value for every dimension mostly in qualitative data obtained, and each variation indicates the ambiguity of every dimension. Equation (2) requires that μtx and μty indicate the center dimensions of a box within the matrix, which is then interpreted as variables within zero and one using the sigmoid activation function in (4). The deviations of every vector in (3) are likewise analyzed using a nonlinear activation function as quantities between zero and just one. The dimensions of a box are handled in YOLOv3 using the tw, th, box before, and logarithmic routines. In alternative terms, the variables of μtw and μth in (2), which represent the tw, th of YOLOv3, really aren't treated as logistic processes since they might have had both favorable and unfavorable quantities. The box parameters of the YOLOv3 sensor level displayed in Figure 1a are solely applicable to solitary Gaussian simulations for forecasting ambiguity. As a result, the method's total computing cost doesn't rise considerably. YOLOv3 needs 99.04 109 FLOPs for just a 512 x 512 intake frequency with ten categories; but, following one Gaussian simulation for each box, 99.04 109 FLOPs are needed. As a result, the charge for classification performance is incredibly modest considering the calculation price rises just by 0.04 percent when related to before simulation.

2.5 Validation in utilizing Localization

Figure 9 depicts the link amongst the IOU as well as the box's clustering ambiguity for such KITTI but also BDD regarding aspects. The findings are presented for vehicles, which have been the dominating category throughout all information, as well as the suggested technique is used to forecast the clustering error. To demonstrate a common propensity, the IOU is split into 0.1 intervals, as well as the mean price of an IOU as well as the approximate amount of a clustering ambiguity are computed and utilized as a standard of reference for every region. Across both samples, as seen in Figure 3, the IOU ratio appears to be growing when the clustering ambiguity reduces. A greater IOU implies that perhaps the anticipated box's dimensions are nearer to those of the GT. Depending on such findings, the suggested individual's clustering ambiguity accurately expresses the anticipated box's reliability. By exploiting the clustering risk anticipated either by suggested methods, it is feasible to deal with mislocalizations and enhance precision.

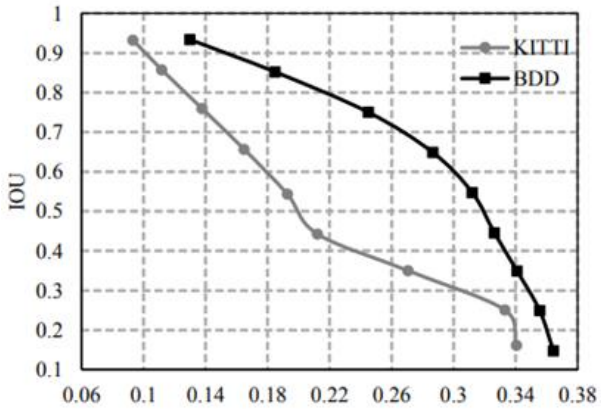

Figure 12 IOU versus localization uncertainty

2.6 Performance evaluation of GAUSSIAN YOLOv3

The approach is tested and alternative approaches utilizing the KITTI classification method are shown in Table 2. The suggested approach, Gaussian YOLOv3, does have a 3.09 improvement in mAP over YOLOv3, as well as the prevention activities is 43.13 fps, allowing for actual identification with a little variation from YOLOv3. Even though Gaussian YOLOv3 is 3.93 fps quicker than RFBNet, which will have the quickest system efficiency across the prior research apart from YOLOv3, the mAP of Gaussian YOLOv3 outperforms RFBNet by even more than 10.17. Furthermore, while the mAP of Gaussian YOLOv3 with either a 512 x 512 granularity is 1.81 less than those of SINet, which would have the best precision amongst preceding approaches, the fps of such suggested protocol is 1.8-times higher. Even though there is an exchange among precision as well as affected productivity, for just a similarity measure, the suggested computation intake granularity is modified and assessed using SINet's fps. The test findings demonstrate that perhaps the mAP of Gaussian YOLOv3 with such a granularity of 704 x 704 displayed mostly in the final row of Table 2 is 86.79 at 24.91 fps, outperforming SINet in high precision overall affected productivity. Table 3 compares the effectiveness of the recommended technique to that of existing approaches on the BDD testing sample. When contrast to YOLOv3, Gaussian YOLOv3 enhances the mAP by 3.5, as well as the control and prevention is 42.5 fps, which is about the similar to YOLOv3. Furthermore, Gaussian YOLOv3 is 3.5 fps quicker than RFBNet, which would have the quickest operating rate amongst some of the prior research save for YOLOv3, notwithstanding Gaussian YOLOv3's precision exceeding RFBNet with 3.9 mAP. Furthermore, when contrasted to CFENet, which would have the higher precision of said conventional techniques, the effectiveness of Gaussian YOLOv3 with such a 736 x 736 source settlement during the last row of Table 3 provides a positive mAP of 1.7 but also speedier procedure pace of 1.5 fps, and thus Gaussian YOLOv3 outshines CFENet in maximum accuracy and affected productivity. Moreover, the AP of Gaussian YOLOv3 mostly on the COCO dataset is 36.1, which would be 3.1 greater than YOLOv3. The AP75 (precise measure) of Gaussian YOLOv3 is 39.0, which itself is 4.6 greater than those of YOLOv3. These findings show that the suggested approach beats YOLOv3 along with KITTI but also BDD in generic datasets. Depending on such test findings, Gaussian YOLOv3 is preferable to the prior techniques since the suggested method may greatly enhance precision while incurring low loss in performance when related to YOLOv3.

Table 1: Average precision (%)

Detection algorithm	Car			Pedestrian			Cyclist			mAP(%)	FPS	Input size
	E	M	H	E	M	H	E	M	H			
MS-CNN	92.54	90.49	79.23	87.46	81.34	72.49	90.13	87.59	81.11	84.71	8.13	1920×576
SINet	99.11	90.59	79.77	88.09	79.22	70.30	94.41	86.61	80.68	85.42	23.98	1920×576
SSD	88.37	87.84	79.15	50.33	48.87	44.97	48.00	52.51	51.52	61.29	28.93	512×512
RefineDet	98.96	90.44	88.82	84.40	77.44	73.52	86.33	80.22	79.15	84.36	27.81	512×512
CFENet	90.33	90.22	84.85	-	-	-	-	-	-	-	0.25	-
RFBNet	87.41	88.35	83.41	65.85	61.30	57.71	74.46	72.73	69.75	73.44	39.20	512×512
YOLOv3	85.68	76.89	75.89	83.51	78.37	75.16	88.94	80.64	79.62	80.52	43.57	512×512
Gaussian YOLOv3	90.61	90.20	81.19	87.84	79.57	72.30	89.31	81.30	80.20	83.61	43.13	512×512
Gaussian YOLOv3	98.74	90.48	89.47	87.85	79.96	76.81	90.08	86.59	81.09	86.79	24.91	704×704

Table 2: Performance comparison using KITTI validation set. E, M, and H refer to easy, moderate, and hard, respectively.

Detection algorithm	mAP(%)	FPS	Input size
MS-CNN	5.7	6.0	1920×576
SINet	9.0	18.2	1920×576
SSD	14.1	23.1	512×512
RefineDet	17.4	22.3	512×512
CFENet	19.1	21.0	512×512
RFBNet	14.5	39.0	512×512
YOLOv3	14.9	42.9	512×512
Gaussian YOLOv3	18.4	42.5	512×512
Gaussian YOLOv3	20.8	22.5	736×736

Table 3: Performance comparison using BDD test set.

	YOLOv3	Gaussian YOLOv3	Variation rate (%)
KITTI validation set			
# of FP	**1,681**	**985**	**-41.40**
# of TP	**13,575**	**14,560**	**+7.26**
# of GT	**17,607**	**17,607**	**0**
BDD validation set			
# of FP	**86,380**	**51,296**	**-40.62**
# of TP	**57,261**	**59,724**	**+4.30**
# of GT	185,578	185,578	0

2.7 Visual and numerical evaluation of FP AND TP

Figures 10 and 11 illustrate recognition instances of either the background with Gaussian YOLOv3 for such KITTI confirmation dataset as well as the BDD test images, correspondingly, for just a subjective observation of Gaussian YOLOv3. The recognition TH is 0.5, which would be the YOLOv3 standard testing TH. The findings in Figure 10's first row and Figure 11's first column indicate how Gaussian YOLOv3 might identify things that YOLOv3 lacks, raising the TP. These favorable findings have been found since the Gaussian modeling plus transfer functions rebuilding of YOLOv3 suggested in this article may give a deficit mitigation impact as in training experience, hence improving training precision for a box but also objectness efficiency. The findings mostly in the second row and second column of Figure 5 reveal that Gaussian YOLOv3 may supplement YOLOv3's inaccurate entity recognition rate. Furthermore, the findings in the third row of Figure 10 and thus the third column of Figure 12 indicate that Gaussian YOLOv3 may reliably determine a box of an item that YOLOv3 has identified incorrectly. According to these findings, Gaussian YOLOv3 may dramatically lower the FP while increasing the TP, improving operating performance and security while preventing catastrophic mishaps. Table 4 provides the counts of FPs as well as TPs for such background and Gaussian YOLOv3 for a mathematical analysis of the FP but also TP of Gaussian YOLOv3. The detecting TH is as previously indicated. Since the GT is supplied throughout the testing dataset, the FP and TP are calculated using the KITTI as well as BDD testing models. Since the KITTI legal assessment approach somehow doesn't include the FP whenever the box is inside a specific size, the FP and TP of the different records are computed by applying the included program of BDD for yet more precise assessments. When contrasted to YOLOv3, Gaussian YOLOv3 lowers the FP by 41.40 percent but also 40.62 percent for such KITTI as well as BDD regarding aspects, correspondingly. Furthermore, it raises the TP by 7.26 percent and 4.3 percent, correspondingly. It must be emphasized that lowering the FP minimizes excessive sudden deceleration, while raising the TP avoids deadly mishaps caused by obstacle identification mistakes. Finally, Gaussian YOLOv3 outperforms YOLOv3 in either FP or TP relating towards the security of driverless driving.

Figure 13 Detection results of the baseline and proposed algorithms

The first column shows the detection results of YOLOv3, whereas the second column shows the detection results of Gaussian YOLOv3.

Figure 14 Detection results of the baseline and proposed algorithms

The first and second rows show the detection results of YOLOv3 and Gaussian YOLOv3, respectively, and each color is related to a particular object class.

2.8 Backbone Networks

In theory, the simplest technique to condense a system would be to lower its abundance and utilize a short computational model. The recognition effectiveness of simplistic systems, on the other hand, is significantly worse than those of machine learning. As a result, this report opts for such strategy of rebuilding the system structure in order to condense the mesh topology. That really is, M-feature YOLO's recovery system is indeed the MobileNet v2 connection. Table 1 depicts the MobileNet v2 routing path. MobileNet v2 is a compact system that could still lower the cost of the algorithm of variables and simulations. Figure 12 depicts the barrier level from the preceding table.

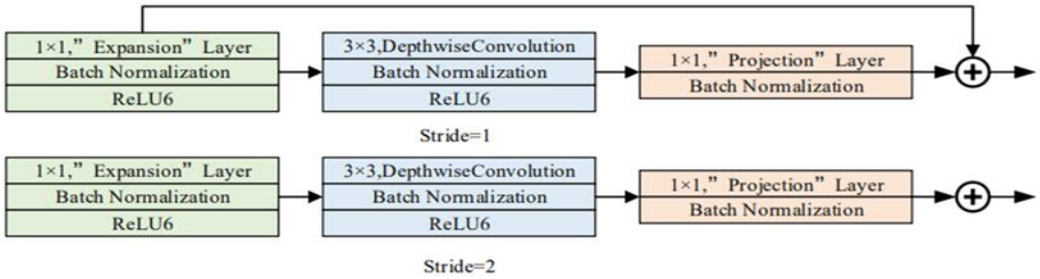

Figure 15 the barrier level from the preceding table.

Figure 15. Bottleneck of MobileNet v2

Input	Operator	t	c	n	s
$224^2 \times 3$	conv2d	-	32	1	2
$112^2 \times 32$	bottleneck	1	16	1	1
$112^2 \times 16$	bottleneck	6	24	2	2
$56^2 \times 24$	bottleneck	6	32	3	2
$28^2 \times 32$	bottleneck	6	64	4	2
$14^2 \times 64$	bottleneck	6	96	3	1
$14^2 \times 96$	bottleneck	6	160	3	2
$7^2 \times 160$	bottleneck	6	320	1	1
1×1×1280	conv2d 1×1	-	k	-	

Table 1. Overall structure of MobileNetV2

2.9 Anchor Boxes

Mostly on training data, the creator of YOLO v3 employed the k-means clustering approach, picking 9 clusters and splitting those into three categories to forecast three sorts of objectives: giant, moderate, as well as tiny. However, the COCO time series contains a minimum of 80 classifications, ranging from little items like tweezers or rodents to enormous items like couches, animals, even railroads. This report, on the other hand, solely identifies automobiles and therefore is separated into two classifications: automobiles and non-vehicles. As a result, the anchor boxes grouped as per the train set are inapplicable towards this report. A classic clustering technique is the k-means method, that finds the ideal K cluster centres by reducing the proximity between both the specimen as well as the data point. The k-means technique is being applied in the report to re-cluster the information presented in this report in order to produce updated anchor boxes. (30,25), (42,34), (51,37), (54,43), (62,50), (72,49), (79,59), and (91,69) are the resultant anchor boxes (120,85).

Chapter 3: SYSTEM ANALYSIS AND DESIGN.

3.1 System Features or Functional Requirements

3.1.1 Introduction

It is critical for a driverless car to identify items in its surroundings in order to function properly. This report discusses how to identify and analyze things to aid driverless cars. Among the most significant conditions for driver assistance systems in driverless cars is the duty of image classification. Deep learning, several of the machine learning jobs, performs image classification much more successfully than previous approaches, and indeed the scope of this study is to recognize items such as automobiles, people, traffic signals, and so forth. Throughout this report, we look at a deep learning technique to entity recognition that predicts the bounding box of an appearance. The process of recognizing things in an input dataset is known as image classification

3.1.2 Input

Vehicle, Image, Driverless, Lane

The system should be completely configured before the usage, and even the consumer has to be familiar with relevant structure. Whenever the construction is ready, you must save it prior to departing so that the core may be piled for future use. The standard has indeed been raised.

3.1.3 Processing/Flowchart

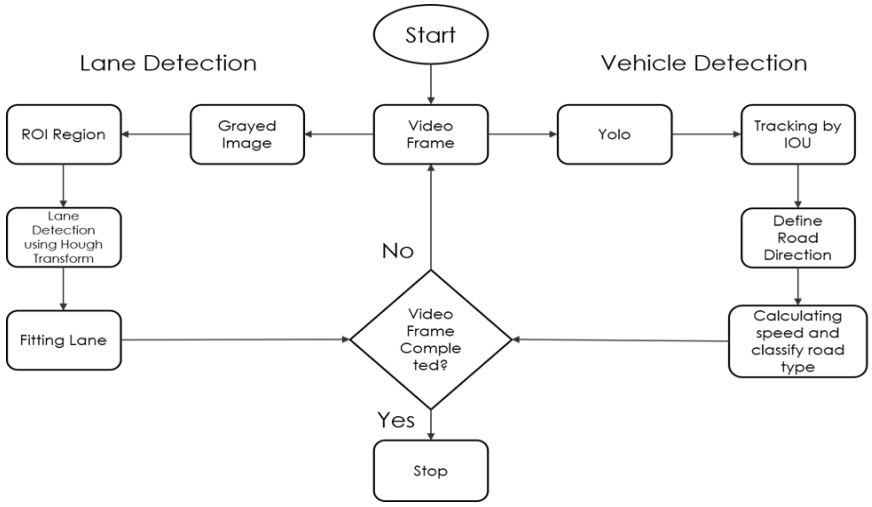

Figure 16 Flowchart of System

3.1.4 Algorithm

1. Convert original image to grayscale.
2. Darkened the grayscale image (this help in reducing contrast from discolored regions of road)
3. Convert original image to HLS colour space.
4. Isolate yellow from HLS to get yellow mask. (For yellow lane markings)
5. Bit-wise OR yellow and white masks to get common mask.
6. Bit-wise AND mask with darkened image .
7. Apply slight Gaussian Blur.
8. Apply canny Edge Detector (adjust the thresholds — trial and error) to get edges.
9. Define Region of Interest. This helps in weeding out unwanted edges detected by canny edge detector.
10. Retrieve Hough lines.
11. Consolidate and extrapolate the Hough lines and draw them on original image.

3.2 The implementation on Lane Detection Using Hough Transform

The "Draw Lines()" vector illustration method is used to link the intersection points for every carriageway (left or right) to form a single straight edge that follows the real traffic inside the photos. The horizontal lines are then generated using the Hough transform, as seen in Fig. 14, and thus are connected mostly by the "Draw Lines()" method to look such as the counterparts in Figs. 15 and 16.

The method does this by doing the proper procedures:

1) Orientation (Left or Right), Every Hough horizontal line is classified as belonging towards the left or right sections. This would be done depending on just the online sector's inclination. Unless the gradient is high somewhere between 0.4 and 1.0, the sector comes to that same left linear category; if this is low and between -0.4 and -1.0, the sector falls to that same right line group.

2) The durations and detects (pedestrian crossings only with x-axis) of all categorized Left as well as Right splices are computed and saved, together with respective gradients.

3) For every class (Left and Right), a line fitting approach is performed, with the gradient of every vertical line indicating whether the vertical line is excellent or poor (sound).

4) The Left and Right arcs may still be produced although to decrease distortion, the data from the image sequences are used to create an Nth order screen (which has already been tested).

5) The FIR filter formula used in this version seems to be as follows:

$$Yk = a0 * Xk + a1 * Xk - 1 + a2 * Xk - 2 + a3 * Xk - 3 + \cdots .. an * Xk - n \quad (8)$$

Table 1 shows the resulting FIR filter settings and factors utilized in this design.

Parameters	Value
Order	7
A_0	0.075
A_1	0.125
A_2	0.175
A_3	0.250
A_4	0.175
A_5	0.125
A_6	0.075

6) By using data of "the feature map" determined in step 5 of the process (V), the gradients and detects of the consequent endpoints are designed to characterize the left line in blue as well as the right line in red.

Figure 17 The image with Hough line segments

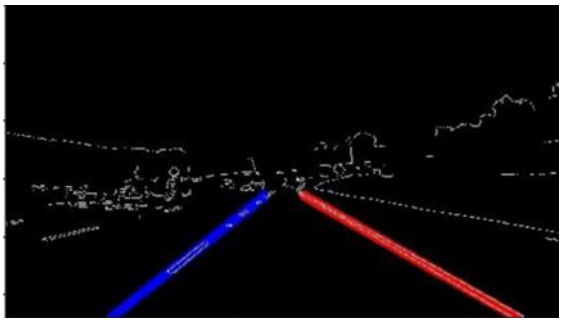

Figure 18 The image after drawing lane lines (blue and red) by extrapolating the Hough lines segments.

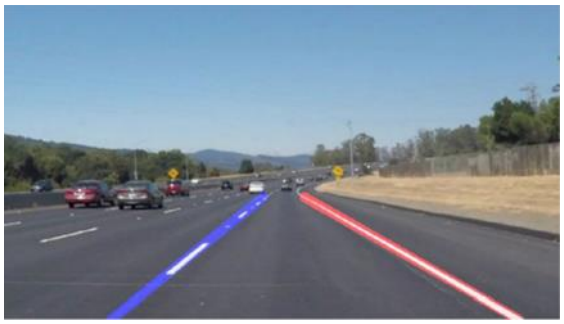

Figure 19 The image after drawing lane lines (blue and red) by extrapolating the Hough lines segments.

3.3 The implementation on Vehicle detection using YOLOv3

Merge of the 3 techniques

- The below image shows a combination of three methodologies to produce the last detection result.
- To split the picture Grid cells are used. In every grid cell, B bounding boxes are projected, along with their reliability or best output score. The class probability of the cell is estimated to identify each item class.
- At least three various types of objects are identified, including a truck, a dog, and a bicycle. To construct all of the projections at the same time A single convolutional neural network is used. When IOU is utilized, the object's bounding box boxes are just like the object's actual boxes. This phenomenon eliminates any unnecessary bounding boxes that do not correspond to the attributes of

the items (like height and width). The end detection will consist of separate bounding boxes that are tailored to the objects.

3.4 Code: -

```
import matplotlib.pylab as plt
import cv2
import numpy as np

car_cascade = cv2.CascadeClassifier('carx.xml')

def region_of_interest(img, vertices):
    mask = np.zeros_like(img)
    # channel_count = img.shape[2]
    match_mask_color = 255
    cv2.fillPoly(mask, vertices, match_mask_color)
    masked_image = cv2.bitwise_and(img, mask)
    return masked_image


def draw_the_lines(img, lines):
    img = np.copy(img)
    blank_image = np.zeros((img.shape[0], img.shape[1], 3), dtype=np.uint8)

    for line in lines:
        for x1, y1, x2, y2 in line:
            cv2.line(blank_image, (x1, y1), (x2, y2), (0, 220, 0), thickness=4)

    img = cv2.addWeighted(img, 0.8, blank_image, 1, 0.0)
    return img

def process(image):
    #image = cv2.imread("road.jpg")
    #image = cv2.cvtColor(image, cv2.COLOR_BGR2RGB)
    #print(image.shape)
    height = image.shape[0]
    width = image.shape[1]

    region_of_interest_vertices = [# to be adjusted as per the image or road, i.e. till road's extreme vertices
        (0, height),
        (0.5*width , 0.5*height),
        (width, height)
    ]
    gray_image = cv2.cvtColor(image, cv2.COLOR_RGB2GRAY)
    canny_image = cv2.Canny(gray_image, 100, 120)
    cropped_image = region_of_interest(canny_image,
                                       np.array([region_of_interest_vertices], np.int32))
    lines = cv2.HoughLinesP(cropped_image,
                            rho=2,
                            theta=np.pi/180,
                            threshold=50,
                            lines=np.array([]),
                            minLineLength=40,
                            maxLineGap=1)
```

```
    image_with_lines = draw_the_lines(image, lines)
    return image_with_lines

cap = cv2.VideoCapture('car_view.mp4')

while(True):

    ret, frame = cap.read()
    frame = process(frame)
    gray = cv2.cvtColor(frame, cv2.COLOR_BGR2GRAY)
    cars = car_cascade.detectMultiScale(gray, 1.1, 3)
    for (x, y, w, h) in cars:
        cv2.rectangle(frame, (x, y), (x + w, y + h), (0, 0, 255), 2)
    cv2.imshow('frame',frame)

    if cv2.waitKey(1) & 0xFF == ord('q'):
        break

cap.release()
cv2.destroyAllWindows()


#plt.imshow(canny_image)
#plt.imshow(cropped_image)
#plt.imshow(image)
#plt.imshow(image_with_lines)
#plt.show()
```

3.5 Validation and Testing

The images of the indicated lane lines are forwarded to the upgraded yolov3 method circuit for retraining. The images employed in the tutorial mode are 416 By 416 px in dimension. Numerous essential indices variables within the method get constantly stored throughout the testing period. Figure 17 depicts the evolution of a standardized incidence functional L value. Figure 17 shows that perhaps the failure optimal value is around 1.8 somewhere at the start of retraining. The closure of such failure evaluation function drops as the number of classes grows, and once the computation time is around 20000, this same depreciation rate is 0.1 left as well as the right to obtain the intended impact.

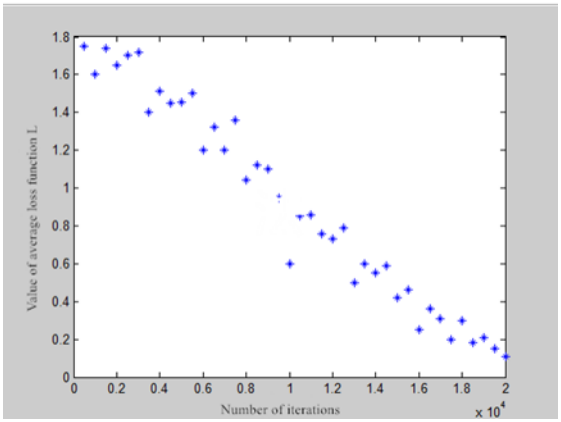

Figure 20 Variation Trend of average loss function value

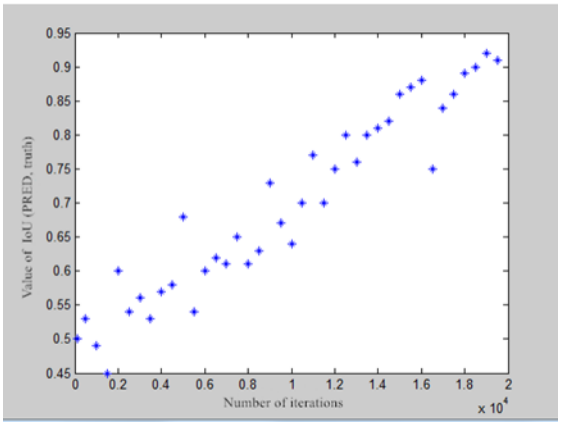

Figure 21 Change trend of matching degree value

Following the example education and experience, 100 straight boundary photographs are examined to see if the software can effectively recognize the lines on the road in the images. Figure 19 depicts the platform's lab results across various changes experienced.

Figure 22 System tests in different external conditions

Chapter 4: RESULTS / OUTPUTS

Sample Name	No. of Frames	Total time Sec	Frame Per Sec
SolidYellowLeft Video	682	48.0	18.76
SolidWhiteRight Video	222	8.0	25.6
Challenge Video	251	23	10.9

The outcomes of videos labeled Clip:1 which carry linear road, Clip:2 which carry curved road, Clip:3 carry a mixture of straight and curved road, and Clip:4 which carry curved road, and so on are shown in the pictures below.

Class: 0	Class: 1
LANE DETECTED:	NOT DETECTED:
.....	.....
tp: 4	tp: 119
fp: 5	fp: 0
tn: 119	tn: 4
fn: 0	fn: 5
pos: 4	pos: 124
neg 124	neg 4
n 128	n 128
Recall (Sensitivity, TPR, Hit Rate): 1.0	Recall (Sensitivity, TPR, Hit Rate): 0.9596774193548387
Specificity (Selectivity, TNR): 0.9596774193548387	Specificity (Selectivity, TNR): 1.0
Precision (Positive Predictive Value): 0.4444444444444	Precision (Positive Predictive Value): 1.0
Negative Predictive Value (NPV): 1.0	Negative Predictive Value (NPV): 0.4444444444444
False Positive Rate (FPR)(Fall-Out): 0.04032258064516129	False Positive Rate (FPR)(Fall-Out): 0.0
False Negative Rate (FNR)(Miss-Out): 0.0	False Negative Rate (FNR)(Miss-Out): 0.04032258064516129
Accuracy: 0.9609375	Accuracy: 0.9609375
fscore: 0.6153846153846154	fscore: 0.9794238683127572
False Discovery Rate (FDR): 0.55555555555555	False Discovery Rate (FDR): 0.0
False Omission Rate (OMR): 0.0	False Omission Rate (OMR): 0.55555555555555

Figure 23 Result of CLIP:1

Class: 0	Class: 1
LANE DETECTED:	NOT DETECTED:
.....	.....
tp: 2	tp: 106
fp: 7	fp: 6
tn: 106	tn: 2
fn: 6	fn: 7
pos: 8	pos: 113
neg 113	neg 8
n 121	n 121
Recal(Sensitivity, TPR, Hit Rate): 0.25	Recal(Sensitivity, TPR, Hit Rate): 0.9380530973451328
Specificity (Selectivity, TNR): 0.9380530973451328	Specificity (Selectivity, TNR): 0.25
Precision (Positive Predictive Value): 0.2222222222222	Precision (Positive Predictive Value):0.9464285714285714
Negative Predictive Value (NPV): 0.9464285714285714	Negative Predictive Value (NPV): 0.2222222222222
False Positive Rate (FPR)(Fall-Out): 0.61946902654867256	False Positive Rate (FPR)(Fall-Out): 0.61946902654867256
False Negative Rate (FNR)(Miss-Out): 0.75	False Negative Rate (FNR)(Miss-Out): 0.75
Accuracy: 0.8925619834710744	Accuracy: 0.8925619834710744
fiscore: 0.23629411764705882	fiscore: 0.9444444444444444
False Discovery Rate (FDR): 0.7777777777778	False Discovery Rate (FDR): 0.05357142857142857
False Omission Rate (OMR): 0.05357142857142857	False Omission Rate (OMR): 0.7777777777778

Figure 24 Result of CLIP:2

Class: 0	Class: 1
LANE DETECTED:	NOT DETECTED:
.....	.....
tp: 1	tp: 93
fp: 5	fp: 5
tn: 93	tn: 1
fn: 5	fn: 5
pos: 6	pos: 98
neg 98	neg 6
n 104	n 104
Recall (Sensitivity, TPR, Hit Rate): 0.1666666666666666	Recall (Sensitivity, TPR, Hit Rate): 0.9489795918367347
Specificity (Selectivity, TNR): 0.9489795918367347	Specificity (Selectivity, TNR): 0.1666666666666666
Precision (Positive Predictive Value): 0.1666666666666666	Precision (Positive Predictive Value): 0.9489795918367347
Negative Predictive Value (NPV): 0.9489795918367347	Negative Predictive Value (NPV):0.1666666666666666
False Positive Rate (FPR)(Fall-Out): 0.0510204081632653 1	False Positive Rate (FPR)(Fall-Out): 0.833333333333333
False Negative Rate (FNR)(Miss-Out): 0.8333333333333334	False Negative Rate (FNR)(Miss-Out): 0.0510204081632653 1
Accuracy: 0.9038641538461539	Accuracy: 0.9038641538461539
fiscore: 0.16666666666666666	fiscore: 0.9489795918367347
False Discovery Rate (FDR): 0.8333333333333334	False Discovery Rate (FDR): 0.0510204081632653 1
False Omission Rate (OMR): 0.0510204081632653 1	False Omission Rate (OMR): 0.8333333333333334

Figure 25 Result of CLIP:3

Class: 0	Class: 1
LANE DETECTED:	NOT DETECTED:
.....	.....
tp: 1	tp: 93
fp: 5	fp: 5
tn: 93	tn: 1
fn: 5	fn: 5
pos: 6	pos: 98
neg 98	neg 6
n 104	n 104
Recall (Sensitivity, TPR, Hit Rate): 0.1666666666666666666	Recall (Sensitivity, TPR, Hit Rate): 0.9489795918367347
Specificity (Selectivity, TNR): 0.9489795918367347	Specificity (Selectivity, TNR): 0.1666666666666666666
Precision (Positive Predictive Value): 0.1666666666666666666	Precision (Positive Predictive Value): 0.9489795918367347
Negative Predictive Value (NPV): 0.9489795918367347	Negative Predictive Value (NPV):0.1666666666666666666
False Positive Rate (FPR)(Fall-Out): 0.05102040816326531	False Positive Rate (FPR)(Fall-Out): 0.833333333333333
False Negative Rate (FNR)(Miss-Out): 0.8333333333333334	False Negative Rate (FNR)(Miss-Out): 0.05102040816326531
Accuracy: 0.9038641538461539	Accuracy: 0.9038641538461539
fiscore: 0.166666666666666666	fiscore: 0.9489795918367347
False Discovery Rate (FDR): 0.8333333333333334	False Discovery Rate (FDR): 0.05102040816326531
False Omission Rate (OMR): 0.05102040816326531	False Omission Rate (OMR): 0.83333333333333334

Figure 26 Result of CLIP:4

Result Output

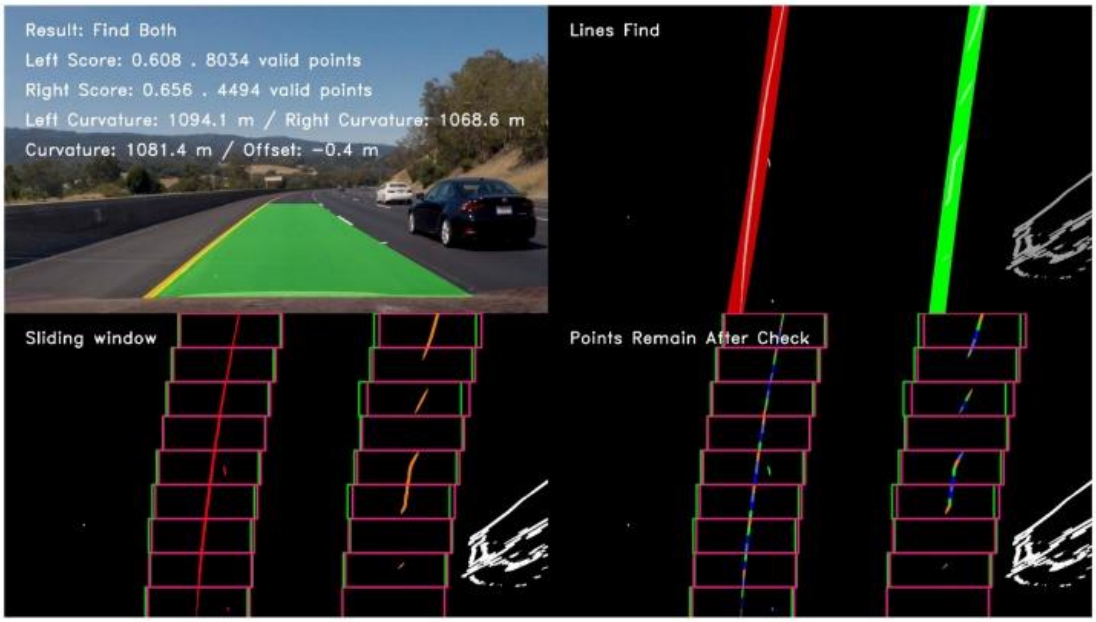

Figure 27 The test result of a typical detected frame in the highway driving video

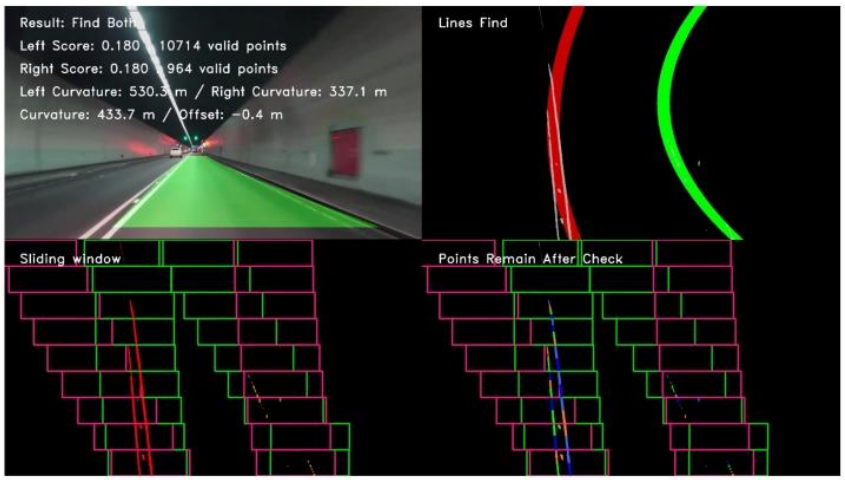

Figure 28 The test result of a typical detected frame in the tunnel road driving video.

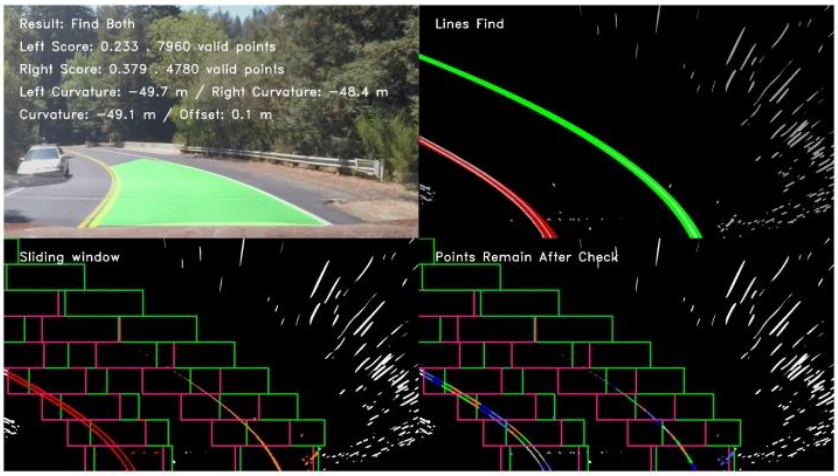

Figure 29 The test result of a typical detected frame in the mountain road driving video

Chapter 5: Conclusion

The assessment of travel demand factors is indeed a critical component of roadway construction and management, and also signalized intersections measures for current facilities. Various methods, including those of static location monitoring and "sensor automobile information" devices, could be used to gather traffic information. Furthermore, Wardrop's moving observer method (MOM) may be employed as a traffic information acquisition approach. Although as usually recognized, artificial intelligence (AI) with deep learning (DL) are widely employed in a wide range of real scenarios, notably automobile classification and tracking. In order to address the issue that standard border tracking algorithms need not take recognition rate and productivity is affected into account, this work proposes a protection system adaptive routing yolov3 approach. Below are the primary enhancements:

1. Based on the features of traffic line pictures' uneven transverse and longitudinal dispersion frequency, it really is recommended to partition the pictures across s * 2S squares to increase height recognition intensity.
2. The sensor size has been limited to four sensor scales: 13 * 13, 26 * 26, 52 * 52104 * 104, which is more suited for detecting tiny objects also including lane dividers.
3. The basic yolov3 device's fully connected layers are reduced from 53 to 49 tiers, simplifying the system and improving system efficiency.
4. Parameters including such closest cluster location and transfer functions have been modified, making them more meaningful and suited for traffic line recognition environments. The real test results reveal that perhaps the revised method has high detection accuracy while identifying level roads, however, the identification is easily influenced whenever the roadways have considerable gradients. As a result, the next report will concentrate on fixing the situation of lane line recognition in huge gradient sceneries.

An image recognition computation, exceptional precision as well as authentic affected productivity are critical for such security plus direct control of driverless cars. Several research on sensor driverless cars have indeed been done, but the results have indeed been unimpressive due to an exchange involving precision and operating efficiency. As a result, this work provides an image processing and analysis method for driverless cars which delivers the optimal exchange among precision and reliability. The suggested technique minimizes errors, boosts TP, and considerably

decreases FP whilst keeping authentic potential using Gaussian simulation, gradient descent rebuilding, including the use of clustering ambiguity. . The suggested Gaussian YOLOv3 approach enhances the mAP by 3.09 but also 3.5 for such KITTI as well as BDD samples, correspondingly, as related to the background. Moreover, since the suggested technique seems to have a better precision than earlier research with comparable fps, it is indeed a good exchange among precision and affected productivity. As a consequence, the suggested method has the potential to considerably enhance the camera-based target recognition technology for driverless cars, and this is projected to contribute heavily to the widespread usage of self-driving technologies. This research offers M-YOLO, a deep learning models approach that relies on YOLO v3. M – YOLO's feature recovery backbone network is based on the MobileNet v2 infrastructure. The level unique version offered by the MobileNet system could significantly minimize the number of variables as well as the complexity of the simulation. The detecting component continues to rely on YOLO v3's multi-scale different recommendation engine. Simultaneously, the K-means technique is utilized in this study to re-cluster the information in order to produce the anchor boxes that are appropriate for this report. Furthermore, M-YOLO employs the EIoU gradient descent to constantly refine the system. According to the statistics, M-average YOLO's detection performance may approach 94.96%, including low-light conditions, the fps could exceed 10.

References

[1] Zhang, Xiang, Wei Yang, Xiaolin Tang, and Jie Liu. "A fast-learning method for accurate and robust lane detection using two-stage feature extraction with YOLO v3." Sensors 18, no. 12 (2018): 4308.

[2] Huang, Shan, Ye He, and Xiao-an Chen. "M-YOLO: A Nighttime Vehicle Detection Method Combining Mobilenet v2 and YOLO v3." In Journal of Physics: Conference Series, vol. 1883, no. 1, p. 012094. IOP Publishing, 2021.

[3] Illingworth, John, and Josef Kittler. "A survey of the Hough transform." Computer vision, graphics, and image processing 44, no. 1 (1988): 87-116.

[4] Mukhopadhyay, Priyanka, and Bidyut B. Chaudhuri. "A survey of Hough Transform." Pattern Recognition 48, no. 3 (2015): 993-1010.

[5] Farag, Wael, and Zakaria Saleh. "Road lane-lines detection in real-time for advanced driving assistance systems." In 2018 International Conference on Innovation and Intelligence for Informatics, Computing, and Technologies (3ICT), pp. 1-8. IEEE, 2018.

[6] Farag, Wael. "Real-time detection of road lane-lines for autonomous driving." Recent Advances in Computer Science and Communications (Formerly: Recent Patents on Computer Science) 13, no. 2 (2020): 265-274.

[7] Farag, Wael. "A comprehensive real-time road-lanes tracking technique for autonomous driving." International Journal of Computing and Digital Systems 9, no. 03 (2020).

[8] Šimunović, Bruno. "Detekcija prometne trake." PhD diss., Josip Juraj Strossmayer University of Osijek. Faculty of Electrical Engineering, Computer Science and Information Technology Osijek. Department of Software Engineering. Chair of Visual Computing, 2021.

[9] Ji, Gaoqing, and Yunchang Zheng. "Lane Line Detection System Based on Improved Yolo V3 Algorithm." (2021).

[10] Gothankar, Nikhil, Chandra Kambhamettu, and Paul Moser. "Circular hough transform assisted cnn based vehicle axle detection and classification." In 2019 4th International Conference on Intelligent Transportation Engineering (ICITE), pp. 217-221. IEEE, 2019.

[11] Reddy, D. Ramesh, Chandravathi Chella, K. Bala Ravi Teja, Heera Rose Baby, and

Prakash Kodali. "Autonomous Vehicle Based on Deep Q-Learning and YOLOv3 with Data Augmentation." In 2021 International Conference on Communication, Control and Information Sciences (ICCISc), vol. 1, pp. 1-7. IEEE, 2021

[12] Bimbraw K. Autonomous cars: Past, present and future: A review of the developments in the last century, the present scenario and the expected future of autonomous vehicle technology; Proceedings of the 12th International Conference on Informatics in Control, Automation and Robotics (ICINCO); Alsace, France. 21–23 July 2015; pp. 191–198. [Google Scholar]

[13] Zhu H., Yuen K.V., Mihaylova L., Leung H. Overview of environment perception for intelligent vehicles. IEEE Trans. Intell. Transp. Syst. 2017;18:2584–2601. doi: 10.1109/TITS.2017.2658662. [CrossRef] [Google Scholar]

[14] Andreev S., Petrov V., Huang K., Lema M.A., Dohler M. Dense moving fog for intelligent IoT: Key challenges and opportunities. IEEE Commun. Mag. 2019;57:34–41. doi: 10.1109/MCOM.2019.1800226. [CrossRef] [Google Scholar]

[15] Chen C.J., Peng H.Y., Wu B.F., Chen Y.H. A real-time driving assistance and surveillance system. J. Inf. Sci. Eng. 2009;25:1501–1523. [Google Scholar]

[16] Zhou Y., Wang G., Xu G.Q., Fu G.Q. Safety driving assistance system design in intelligent vehicles; Proceedings of the 2014 IEEE International Conference on Robotics and Biomimetics (IEEE ROBIO); Bali, Indonesia. 5–10 December 2014; pp. 2637–2642. [Google Scholar]

[17] D'Cruz C., Ju J.Z. Lane detection for driver assistance and intelligent vehicle applications; Proceedings of the 2007 International Symposium on Communications and Information Technologies (ISCIT); Sydney, Australia. 16–19 October 2007; pp. 1291–1296. [Google Scholar]

[18] Kum C.H., Cho D.C., Ra M.S., Kim W.Y. Lane detection system with around view monitoring for intelligent vehicle; Proceedings of the 2013 International SoC Design Conference (ISOCC); Busan, Korea. 17–19 November 2013; pp. 215–218. [Google Scholar]

[19] Scaramuzza D., Censi A., Daniilidis K. Exploiting motion priors in visual odometry for vehicle-mounted cameras with non-holonomic constraints; Proceedings of the 2011 IEEE/RSJ International Conference on Intelligent Robots and Systems: Celebrating 50 Years of Robotics (IROS); San Francisco, CA, USA. 25–30 September 2011; pp. 4469–

4476. [Google Scholar]
[20] Li B., Zhang X.L., Sato M. Pitch angle estimation using a Vehicle-Mounted monocular camera for range measurement; Proceedings of the 2014 12th IEEE International Conference on Signal Processing (ICSP); Hangzhou, China. 19–23 October 2014; pp. 1161–1168. [Google Scholar]
[21] Schreiber M., Konigshof H., Hellmund A., Stiller C. Vehicle localization with tightly coupled GNSS and visual odometry; Proceedings of the 2016 IEEE Intelligent Vehicles Symposium (IV); Gotenburg, Sweden. 19–22 June 2016; pp. 858–863. [Google Scholar]
[22] Zhang Y.L., Liang W., He H.S., Tan J.D. Perception of vehicle and traffic dynamics using visual-inertial sensors for assistive driving; Proceedings of the 2018 IEEE International Conference on Robotics and Biomimetics (ROBIO); Kuala Lumpur, Malaysia. 12–15 December 2018; pp. 538–543. [Google Scholar]
[23] Wang J.N., Ma H.B., Zhang X.H., Liu X.M. Detection of lane lines on both sides of road based on monocular camera; Proceedings of the 2018 IEEE International Conference on Mechatronics and Automation (ICMA); Changchun, China. 5–8 August 2018; pp. 1134–1139. [Google Scholar]
[24] Li Y.S., Zhang W.B., Ji X.W., Ren C.X., Wu J. Research on lane a compensation method based on multi-sensor fusion. Sensors. 2019;19:1584. doi: 10.3390/s19071584. [PMC free article] [PubMed] [CrossRef] [Google Scholar]
[25] Zheng B.G., Tian B.X., Duan J.M., Gao D.Z. Automatic detection technique of preceding lane and vehicle; Proceedings of the IEEE International Conference on Automation and Logistics (ICAL); Qingdao, China. 1–3 September 2008; pp. 1370–1375. [Google Scholar]